



**UNIVERSITY OF LEEDS**

This is a repository copy of *The impact of road grade on carbon dioxide (CO<sub>2</sub>) emission of a passenger vehicle in real-world driving*.

White Rose Research Online URL for this paper:  
<http://eprints.whiterose.ac.uk/83026/>

Version: Accepted Version

---

**Article:**

Wyatt, DW, Li, H [orcid.org/0000-0002-2670-874X](http://orcid.org/0000-0002-2670-874X) and Tate, JE [orcid.org/0000-0003-1646-6852](http://orcid.org/0000-0003-1646-6852) (2014) The impact of road grade on carbon dioxide (CO<sub>2</sub>) emission of a passenger vehicle in real-world driving. *Transportation Research Part D: Transport and Environment*, 32. pp. 160-170. ISSN 1361-9209

<https://doi.org/10.1016/j.trd.2014.07.015>

---

**Reuse**

Items deposited in White Rose Research Online are protected by copyright, with all rights reserved unless indicated otherwise. They may be downloaded and/or printed for private study, or other acts as permitted by national copyright laws. The publisher or other rights holders may allow further reproduction and re-use of the full text version. This is indicated by the licence information on the White Rose Research Online record for the item.

**Takedown**

If you consider content in White Rose Research Online to be in breach of UK law, please notify us by emailing [eprints@whiterose.ac.uk](mailto:eprints@whiterose.ac.uk) including the URL of the record and the reason for the withdrawal request.



[eprints@whiterose.ac.uk](mailto:eprints@whiterose.ac.uk)  
<https://eprints.whiterose.ac.uk/>

# The Impact of Road Grade on Carbon Dioxide (CO<sub>2</sub>) Emission of a Passenger Vehicle in Real-World Driving

David W. Wyatt<sup>a\*</sup>, Hu Li<sup>b</sup>, James E. Tate<sup>c</sup>

<sup>a\*</sup> Corresponding author. Doctoral Training Centre in Low Carbon Technologies, University of Leeds, Leeds, LS2 9JT. E-mail address: [pmdww@leeds.ac.uk](mailto:pmdww@leeds.ac.uk) (D.W. Wyatt). Tel.: +44 (0)1133 432556; fax: +44 (0)1132 467310

<sup>b</sup> Energy Research Institute, School of Process, Environment and Materials Engineering, University of Leeds, Leeds, LS2 9JT, UK.

<sup>c</sup> Institute for Transport Studies, University of Leeds, Leeds, LS2 9JT, UK.

## Abstract

To accurately estimate real-world vehicle emission at 1Hz the road grade for each second of data must be quantified. Failure to incorporate road grade can result in over or underestimation of a vehicle's power output and hence cause inaccuracy in the instantaneous emission estimate. This study proposes a simple LiDAR (Light Detection And Ranging) – GIS (Geographic Information System) road grade estimation methodology, using GIS software to interpolate the elevation for each second of data from a Digital Terrain Map (DTM). On-road carbon dioxide (CO<sub>2</sub>) emissions from a passenger car were recorded by Portable Emission Measurement System (PEMS) over 48 test laps through an urban-traffic network. The test lap was divided into 8 sections for micro-scale analysis. The PHEM instantaneous emission model (Hausberger, 2003) was employed to estimate the total CO<sub>2</sub> emission through each lap and section. The addition of the LiDAR-GIS road grade to the PHEM modelling improved the accuracy of the CO<sub>2</sub> emission predictions. The average PHEM estimate (with road grade) of the PEMS measured section total CO<sub>2</sub> emission (n=288) was 93%, with 90% of the PHEM estimates between 80% and 110% of the PEMS recorded value. The research suggests that instantaneous emission modelling with LiDAR-GIS calculated road grade is a viable method for generating accurate real-world micro-scale CO<sub>2</sub> emission estimates. The sensitivity of the CO<sub>2</sub> emission predictions to road grade was also tested by lessening and exaggerating the gradient profiles, and demonstrates that assuming a flat profile could cause considerable error in real-world CO<sub>2</sub> emission estimation.

35 **Keywords**

36

37 Vehicle Emissions; Carbon Dioxide; Vehicle Specific Power; Road Grade; Portable Emission  
38 Measurement System (PEMS); LiDAR.

39

40

41 **1. Introduction**

42

43 Research has demonstrated that on-board vehicle Portable Emission Measurement Systems (PEMS)  
44 can be utilised to provide accurate measurement of vehicle exhaust emissions in real-world driving  
45 (Frey et al., 2003; Liu et al., 2010; Ropkins et al., 2007). PEMS instrumentation in such studies are  
46 deployed to record the motion, geographical position and exhaust emission of a vehicle driven over a  
47 real-world test route, most commonly measured on a second-by-second basis. Utilising the 1Hz  
48 PEMS data and values from the test vehicle specification, the engine power output of the vehicle for  
49 each second of data can be computed and used as an explanatory variable in predicting fuel  
50 consumption and exhaust emission at that instant.

51

52 Exploiting the relationship between engine power and exhaust emission, the latest generation of  
53 emissions models such as the US Environmental Protection Agency's (EPA) MOtor Vehicle Emission  
54 Simulator (MOVES) (Koupal et al., 2004), the Netherlands Organisation for Applied Scientific  
55 Research's (TNO) VERSIT+ model (Smit et al., 2007) and the Technical University of Graz's (TUG)  
56 Passenger car and Heavy duty Emission Model (PHEM) (Hausberger, 2003) predict vehicle exhaust  
57 emission by referencing the calculated engine power output for each second of data to a calibrated  
58 mass of exhaust emission at that power, for each emission species.

59

60 Derivation of instantaneous engine power output requires a second-by-second measure of vehicle  
61 speed, acceleration and road gradient. PEMS can reliably capture vehicle speed, and hence  
62 acceleration, during real-world driving, but road grade is very difficult to measure accurately from an  
63 instrumented vehicle (Zhang and Frey, 2006).

64

65 A number of studies have highlighted the significant influence road grade can have on real-world fuel  
66 consumption and exhaust emission (Boriboonsomsin and Barth, 2009; Boroujeni and Frey, 2014;  
67 Zhang and Frey, 2006). For test sections with positive road grade, as the gradient increases so must  
68 the engine power output to keep the vehicle at a constant speed, due to the increasing force of gravity  
69 opposing the motion of the vehicle. This increase in power requires greater fuel consumption  
70 resulting in increased CO<sub>2</sub> exhaust emission. Likewise where a vehicle is travelling on a road with  
71 negative grade, gravity acts to accelerate the vehicle, reducing the power demand on the engine,

72 which lowers fuel consumption and hence CO<sub>2</sub> emission. Zhang and Frey (2006) recorded an  
73 increase in CO<sub>2</sub> emission of 40-90% for three light duty gasoline vehicles over sections of road with  
74 gradient  $\geq 5\%$  when compared to sections with gradient  $\leq 0\%$ , whilst Boriboonsomsin and Barth  
75 (2009) measured a 15-20% rise in fuel consumption for a gasoline passenger car between a flat route  
76 and a hilly route.

77

78 Given the effect of road grade on engine power output and therefore vehicle emission, it is vital for  
79 micro-scale emission modelling that instantaneous engine power output is calculated accurately,  
80 which necessitates a representative road grade value for each second of test data. There are a number  
81 of methods for quantifying road grade proposed in the literature, including; calculation from design  
82 drawings; direct land survey measurement; on-board measurement by GPS, accelerometers,  
83 barometric altimeters and inclinometers; and mathematical derivation from DTM or DEM (digital  
84 elevation maps), each with different characteristics relating to accuracy, precision, scale and price  
85 (Boroujeni et al., 2013; Sahlholm and Johansson, 2010; Zhang and Frey, 2006). Zhang and Frey  
86 (2006) proposed a LiDAR based methodology concluding that the LiDAR method is advantageous;  
87 having relatively few practical and logistical limitations compared with other methods, and can be  
88 considered sufficiently accurate for emission estimation.

89

90 LiDAR is a mapping technique which quantifies terrain elevation using laser measurement from  
91 aircraft. These measurements can be processed to construct highly accurate Digital Terrain Models  
92 (DTM) which render a three dimensional representation of the surface topography, describing  
93 elevation and position. The availability and cost of LiDAR data have been a cited as a main  
94 limitation in its use for road grade estimation (Boroujeni et al., 2013), however, a comprehensive  
95 LiDAR 5-metre resolution DTM dataset for the U.K. is available free of charge to academics and  
96 students at U.K. institutions through the Landmap Kaia Service hosted at MIMAS based at the  
97 University of Manchester (Millin-Chalabi et al., 2011). The advantage of the simple LiDAR-GIS  
98 method proposed in this study is that by referencing the measured GPS position to a DTM elevation, a  
99 representative 1Hz road grade profile can be quickly generated for a test area without the multiple  
100 runs required by GPS measured altitude methodologies (Boroujeni et al., 2013; Sahlholm and  
101 Johansson, 2010) and without the detailed roadway analysis and segmentation required in the LiDAR  
102 methodology described by Zhang and Frey (2006).

103

104 In combination with reducing the fossil fuel dependence of the vehicle fleet through engine efficiency  
105 improvements and new vehicle technologies, road traffic management schemes may also deliver CO<sub>2</sub>  
106 emission reductions. Mechanisms such as better traffic control systems, which reduce the number of  
107 aggressive braking and acceleration events through a network; eco-driver training, which promotes  
108 efficient driving; policies which reward multiple-occupancy of cars or the use of public transport to

109 reduce both the number of vehicle trips and traffic congestion; and improved road geometry design to  
110 reduce the impact of road grade can all be used to reduce CO<sub>2</sub> emission from the road transport sector.  
111 In order to provide detailed micro-scale assessment of the impact of such strategies, emission  
112 estimation models are required that can predict emissions of vehicles in real-world driving conditions  
113 with sufficient accuracy and resolution to quantify their environmental benefit and inform the policy  
114 decision making process.

115

116 The purpose of this paper is to develop and demonstrate a simple LiDAR-GIS methodology for  
117 calculating a representative 1Hz road grade for use in instantaneous vehicle emission modelling. The  
118 sensitivity of CO<sub>2</sub> emission predictions to road grade, in a range of traffic conditions will also tested.

119

120

## 121 2. Methodology

122

### 123 2.1. Study Design

124

125 A fixed lap through Headingley, Leeds was used as a test route for the research. This test lap, shown  
126 in Figure 1, comprises a 4.6 km route on mainly single lane urban commuter roads, with a speed limit  
127 of 30 mph (48 km/h). The route encompasses one of the main arterial roads into and out of Leeds and  
128 is frequently congested.

129

130

Figure 1. Headingley Test Lap and Sections (GPSVisualizer, 2013)



131

132

133 The test lap was covered by the same driver in an instrumented vehicle a total of 48 times during a  
134 week-long testing period between the 26<sup>th</sup> February 2007 and the 5<sup>th</sup> March 2007, with runs conducted  
135 between the hours of 07:30 and 21:00 to capture the full range of traffic conditions for this road  
136 network. The laps were completed in variety of weather conditions, with sunny, dry, overcast and  
137 rainy test laps, in temperatures ranging from 1°C to 15°C.

138

139 In order to facilitate analysis at a micro-scale level the Headingley lap was divided into 8 test sections  
140 (see Figure 1). These sections were determined by classifying points of latitude and longitude to mark  
141 the beginning and end of each section, after which the closest measured GPS points from each run to  
142 those selected start and end points were identified. Sections 1 and 8 are the same segment of road but  
143 with opposite directions of traffic flow, likewise sections 2 and 4, and sections 5 and 7. Section 3 and  
144 section 6 are separate short ‘turning’ sections.

145

## 146 2.2. Test Vehicle

147

148 The instrumented vehicle used in this study was a EURO 4 emission compliant petrol Ford Mondeo  
149 with a 5-speed manual gearbox and a port fuel injected 1.8 litre, 4 cylinder, 16 valve spark ignition  
150 engine with a maximum power of 92 kW (125 PS) at 6000 rpm. The vehicle was equipped with a  
151 Three Way Catalyst (TWC).

152

153 The vehicle specifications used for modelling in this study are a kerbweight (with 90% fuel levels, full  
154 fluid levels and a 75kg driver) of 1374 kg (Li et al., 2008), a rolling resistance coefficient of 0.013  
155 (Ehsani et al., 2009), an aerodynamic drag coefficient of 0.32, a frontal area of 2.3 m<sup>2</sup> (Doucette and  
156 McCulloch, 2011), and an idle engine speed of 850 rpm.

157

## 158 2.3. Test Vehicle Instrumentation

159

160 A Horiba On Board emission measurement System (OBS-1300) was used to measure the exhaust  
161 flow rate and air/fuel ratio, enabling calculation of CO<sub>2</sub> mass emission from the volumetric  
162 measurements. Speed, acceleration and geographical position data were measured and recorded by a  
163 RaceLogic VBOX II GPS engine and data logger. All data was recorded at 1 Hz. The OBS set up and  
164 its validation over a wide range of engine operating conditions and drive cycles is described by  
165 Ropkins et al. (2008).

166

167 The OBS and VBOX were time aligned using the vehicle velocity data measured by each instrument.  
168 Exhaust flow measurement drift was corrected, where required, using the standard ‘on-road’  
169 correction method used in other University of Leeds studies, measuring ‘zero flow’ values before and

170 after each test run and re-calibrating the zero-points, assuming a linear drift over the test (Ropkins et  
171 al., 2007). The documented OBS-1300 ‘pulse effect’ overestimation of idle exhaust flow (Daham et  
172 al., 2005; Nakamura et al., 2002; Ropkins et al., 2008) was corrected based on the work of Ropkins et  
173 al. (2008), which demonstrated an OBS overestimation of idle exhaust flow rate in the order of 40 to  
174 60 percent. A correction factor was applied to the OBS measured exhaust flow rate at all points of  
175 vehicle engine idle recorded during the testing.

176

#### 177 2.4. Mass Emission Calculation

178

179 The exhaust CO<sub>2</sub> emissions as measured by use of the OBS-1300 are captured on a volumetric basis.  
180 The CO<sub>2</sub> mass emission rate is calculated from the measured exhaust gas volumetric flow rate, the  
181 density of CO<sub>2</sub> and the wet gas concentration of CO<sub>2</sub>, using Equation 1.

182

$$183 \text{CO}_{2\text{ MASS}} = [\text{CO}_2]_{t=t+\text{DT}} \times \text{MWT}_{\text{CO}_2} \times [\text{Q}_{\text{EX}}]_{t=t} \times (273.15/293.15) \times \text{UCF} \quad (1)$$

184

185 Where, CO<sub>2 MASS</sub> is the CO<sub>2</sub> mass emission rate in g/s, standardised to 20°C and 1 atm (293.15K and  
186 101.3 kPa); [Q<sub>EX</sub>]<sub>t=t</sub> is the exhaust flow rate in m<sup>3</sup>/min at time t; [CO<sub>2</sub>]<sub>t=t+DT</sub> is the percentage  
187 concentration of CO<sub>2</sub> associated with [Q<sub>EX</sub>]<sub>t=t</sub>, which is read after a measurement Delay Time (DT);  
188 MWT<sub>CO<sub>2</sub></sub> is the molecular weight of CO<sub>2</sub>, 44.01 g/mol; and UCF are the required Unit Conversion  
189 Factors. The Unit Conversion Factors are a multiplication by 1/100 to correct the units of [CO<sub>2</sub>]<sub>t=t+DT</sub>  
190 from a percentage volume to volume; a multiplication of 1/60 to change the units of [Q<sub>EX</sub>]<sub>t=t</sub> from  
191 m<sup>3</sup>/min to m<sup>3</sup>/s; a multiplication of 1/22.415 to convert MWT<sub>CO<sub>2</sub></sub> from g/mol to CO<sub>2</sub> density using the  
192 ideal gas volume of 1 mole at Standard Temperature and Pressure (STP), with 273.15/293.15  
193 amending the density of CO<sub>2</sub> to that at 20°C and 1 bar

194

#### 195 2.5. LiDAR-GIS Methodology for Elevation Profile and 1Hz Road Grade Estimation

196

197 The possible error range resulting from instrument imprecision (the VBOX II has a 95% Circular  
198 Error Probability (CEP) of 10 metres, meaning that the measured height is within 10 metres of the  
199 true position 95% of the time (Racelogic, 2008)) and measurement errors during vehicle transit,  
200 caused by GPS signal interference from buildings in urban streets for example, made the raw GPS  
201 height measurements recorded by the instrumented vehicle too unreliable to use to generate an  
202 accurate elevation profile for the test lap, and insufficiently precise to calculate road grade for each  
203 second of data. The test lap elevation profile in this research was instead calculated using a 5m DTM,  
204 generated from the LiDAR elevation data, provided through Landmap Kaia (Millin-Chalabi et al.,

205 2011) . The DTM and the VBOX measured GPS positions for each test run were imported into the  
206 GIS software ArcGIS enabling the height at each recorded GPS point to be extracted from the DTM.  
207

208 The road grade for each second of recorded data was calculated by applying an algorithm to reduce  
209 the effect of errors associated with inaccuracies in the measured GPS latitude and longitude position  
210 (95% CEP of 3m (Racelogic, 2008)). The errors resulting from GPS absolute position measurement  
211 accuracy are especially apparent at points where the vehicle was moving slowly or stationary, as the  
212 GPS position appears to shift whilst the vehicle is not moving. As the GPS position changes, so does  
213 the elevation estimate extracted from the 5-metre DTM and relatively small changes in GPS position  
214 can result in changes in the elevation estimate. Unfeasible erroneous gradients may therefore be  
215 calculated where the vehicle travels only a short distance along the test route but due to GPS  
216 measurement error there is a significant change in the DTM extracted elevation.

217  
218 In order to determine a representative gradient on a second-by-second basis an algorithm was  
219 therefore applied to smooth out the errors resulting from GPS absolute position measurement  
220 imprecision. For each second of data, when the vehicle was travelling at greater than 10m/s then the  
221 gradient was calculated by dividing the distance travelled in the measured second by the change in  
222 height in that measured second. Where the vehicle was travelling at less than 10m/s, rather than  
223 calculating the gradient over 1 second, the gradient is calculated over the period from where the  
224 vehicle was at least 5 metres before the start of that measured second to the point where the vehicle  
225 was at least 5 metres past the end of the measured second. This ensures that the minimum length of  
226 road section over which the gradient is calculated is 10 metres.

227  
228 The Bluesky LiDAR height data utilised in this study have an accuracy of up to  $\pm 10\text{cm}$  (Bluesky,  
229 2013), however the resolution of the DTM does have an influence on the accuracy of LIDAR based  
230 elevation estimates. In this study, the 5-metre resolution DTM presents a map of LiDAR calculated  
231 elevations at the intersection points on a horizontal 5 metre grid covering the test area. The height of  
232 any GPS point within that grid is calculated by linearly interpolating between the nearest grid  
233 intersection points, by the GIS software. However as a result of interpolation, surface features such as  
234 bridges, underpasses and steep road side banking, where there is an abrupt non-linear change in  
235 surface elevation within a 5-metre grid square, can produce errors in the height estimation. In these  
236 cases the modelled linear change in surface height does not reflect the abrupt real-world change.  
237 Manual correction of physically unfeasible road grade estimates could be undertaken utilising geo-  
238 referenced photographic images. In this study no manual adjustments of the estimate road grade were  
239 necessary, as the Headingley test lap contained no surface features that required correction.

240



## 241 2.6. Vehicle Specific Power

242

243 Vehicle Specific Power (VSP) is employed in this research to estimate the power per unit mass for the  
244 vehicle for each second of recorded data. The VSP of the test vehicle was calculated for each second  
245 of test data, from the 1Hz vehicle speed data, recorded by PEMS measurement, and the 1Hz road  
246 grade estimate generated by the LiDAR-GIS methodology. The general form of the VSP equation  
247 (Jimenez-Palacios, 1999) is described in Equation 2.

248

$$249 \text{VSP} = v \cdot (a \cdot (1 + \varepsilon_i) + (g \cdot \text{grade}) + (g \cdot C_R)) + (0.5\rho_a ((C_D \cdot A)/m) (v + v_w)^2 \cdot v) \quad (2)$$

250

251 Where VSP is vehicle specific power (kW/tonne);  $v$  is vehicle speed (m/s);  $a$  is vehicle acceleration  
252 ( $\text{m/s}^2$ );  $\varepsilon_i$  is the gear-dependent “Mass factor” (tonne), which is the equivalent translational mass of  
253 the rotating components of the powertrain;  $g$  is the acceleration of gravity ; grade is road grade  
254 (dimensionless);  $C_R$  is the coefficient of rolling resistance (dimensionless);  $\rho_a$  is the ambient air  
255 density ( $\text{kg/m}^3$ );  $C_D$  is the drag coefficient (dimensionless);  $A$  is the frontal area of the vehicle ( $\text{m}^2$ );  $m$   
256 is the mass of the vehicle and  $v_w$  is the velocity of the headwind into the vehicle.

257

258 For this study the simplified VSP equation for a typical light duty vehicle (Jimenez-Palacios, 1999)  
259 was employed, with the rolling resistance term coefficient ( $g \cdot C_R$ ) of 0.128 and aerodynamic drag  
260 term coefficient ( $0.5\rho_a (C_D \cdot A)/m$ ) of 0.000318 calculated to correspond to the test vehicle used in  
261 the research.

262

$$263 \text{VSP}_{\text{EURO4}} = v \times [(1.1 \times a) + (9.81 \times (\sin(\text{atan}(\text{grade}))) + 0.128] + (0.000318 \times v^3) \quad (3)$$

264

## 265 2.7. Modelling in PHEM

266

267 Vehicle emission estimation in this research was conducted using the power-instantaneous emission  
268 model PHEM (Hausberger, 2003). The PHEM model enables micro-scale calculation of vehicle  
269 second-by-second fuel consumption and exhaust emission in any reasonable driving conditions.

270 PHEM requires a 1Hz speed profile with associated road grade measurements and data describing the  
271 test vehicle to calculate, for each second of test data, the engine speed and power output of the vehicle.  
272 These speed and power values are then referenced to an engine emission map, specific to the test  
273 vehicle’s fuel type and certified EU emission standard, to estimate the second-by-second vehicle fuel  
274 consumption and emission values (Hausberger et al., 2010).

275

276 For this study the 1Hz speed profile from the PEMS was used with LiDAR-GIS calculated road  
277 grades. The specification data (as described in Section 2.2) for the EURO 4 Mondeo test vehicle were  
278 used to parameterise PHEM, with an estimated loading of 150 kg for the PEMS system. The PHEM  
279 engine-emission map used during the modelling was that for a comparable EURO 4 petrol vehicle.  
280  
281

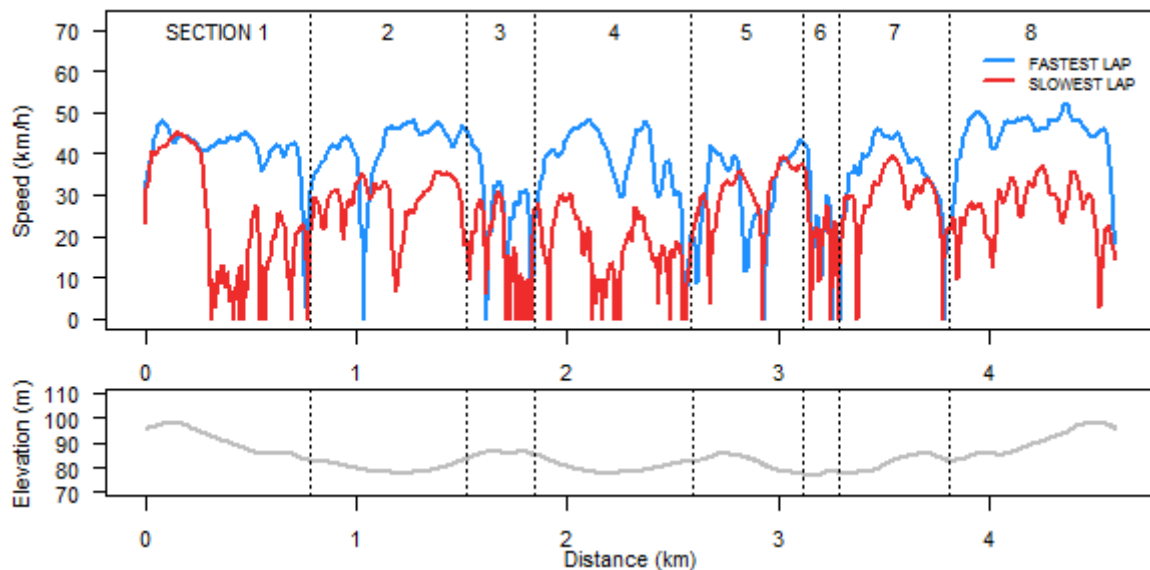
### 282 3. Analysis of PEMS Measurements over the Headingley Test Lap

283

284 The median time to complete the test route over the 48 test laps was 19 minutes 50 seconds, however  
285 the lap times ranged from 10 minutes 14 seconds in free flowing conditions to 28 minutes 37 seconds  
286 in congested traffic. The average lap speed was 14.2 km/h (range 9.6 km/h to 27 km/h). Plotting the  
287 distance - speed profile for the slowest lap, recorded at 8.20am in peak morning rush hour traffic  
288 against the fastest lap, recorded at 8:36pm in free flowing traffic conditions, highlights the variation in  
289 vehicle operation which can occur over the same lap and road segments. The speed profile for the  
290 congested lap, marked in red in Figure 2, displays recurrent periods of very low speed, where the  
291 vehicle frequently stops and starts. Even outside of these periods, congestion hinders the vehicle from  
292 reaching the 48 km/h speed limit for the road. The distance - speed profile for the fastest lap, marked  
293 in blue, shows that whilst there were points where the vehicle was stationary, there were noticeably  
294 fewer stationary points than during slowest lap, and upon restarting the vehicle was able to accelerate  
295 back up to the speed limit of the road.  
296

296

297 Figure 2. (a) Vehicle Distance - Speed Profiles for the Fastest and Slowest Recorded Laps and  
298 (b) Elevation Profile



299  
300

301 The specific traffic conditions experienced during each of the real-world test runs influenced both the  
302 driver input (and as a result engine load) and the total time to complete the lap. The variability of

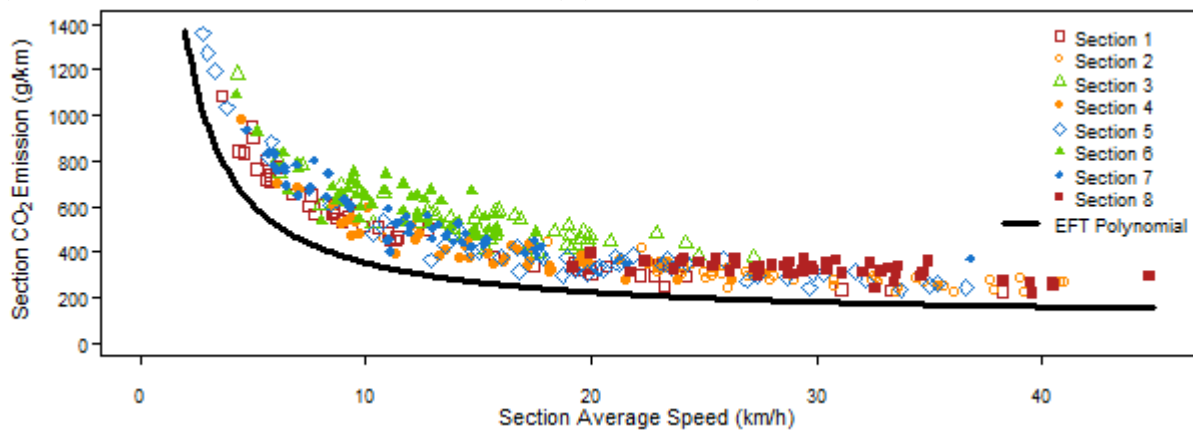
303 these conditions resulted in a wide range of average CO<sub>2</sub> emissions per km for the 48 test laps (313  
304 gCO<sub>2</sub>/km to 586 gCO<sub>2</sub>/km). The median emission over the 48 laps was 438 gCO<sub>2</sub>/km, which is more  
305 than double the rated CO<sub>2</sub> emission for the vehicle of 182 gCO<sub>2</sub>/km (Ford, 2005).

306

307 Figure 3 compares the PEMS measured gCO<sub>2</sub>/km for each of the road sections. Although the section  
308 emissions roughly follow the curve of the EFT function, for this vehicle the function underestimates  
309 the emission generated in every section. It is also clear from the graph that at each speed the real-  
310 world measurements show a wide spread of possible emission rates, indicating that CO<sub>2</sub> emission  
311 assessment through an average speed function may not provide a reasonable estimate for real-world  
312 CO<sub>2</sub> emission in all situations.

313

314 Figure 3. PEMS Measured Section CO<sub>2</sub> Emissions versus Section Average Speed (n=384). EFT  
315 Polynomial is the Emission Factor Toolkit (EFT) average speed emission function for the vehicle type  
316 (R012, Car <2.5 t, Petrol, 1400-2000 cc, Euro 4) (DEFRA, 2009)

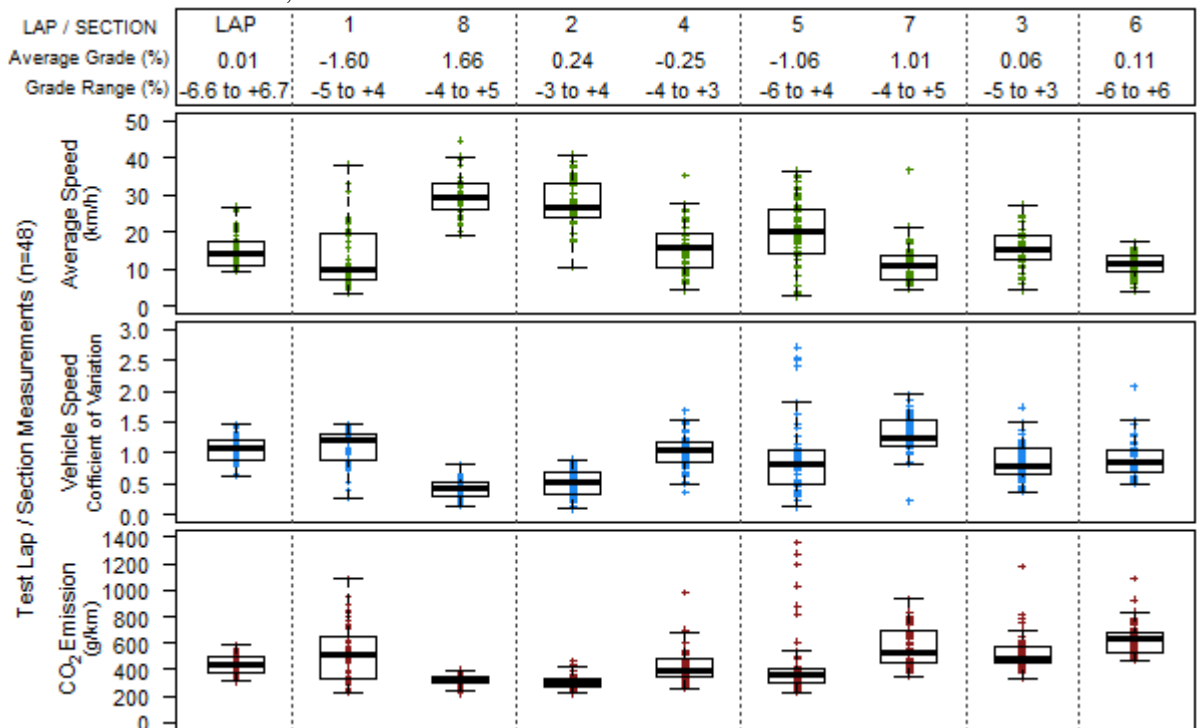


317  
318

319 The coefficient of variation (CV) is the ratio of the standard deviation to the mean, is a measure of the  
320 relative dispersion of vehicle speeds from the average speed, and describes the consistency of the  
321 vehicle speed through a lap or section. A low CV indicates a relatively constant speed and a high CV  
322 shows a wide dispersion of vehicle speeds. Sections 2 and 8 had the lowest rate of CO<sub>2</sub> emission and  
323 also the narrowest spread of emission values (see Figure 4). These were the sections with consistently  
324 high average speeds and relatively consistent vehicle speed. In these sections traffic flow was not  
325 greatly hindered by increased traffic density in the network during peak traffic periods. Conversely  
326 the data for sections 1 and 7 present a wide spread of CO<sub>2</sub> emission values. During free flowing  
327 conditions these sections could be completed relatively quickly, at relatively low gCO<sub>2</sub>/km emission  
328 rates. However, during rush hour periods, the queuing times over these sections increased, raising the  
329 vehicles gCO<sub>2</sub>/km emission rate because the stationary vehicle's idle CO<sub>2</sub> emissions increase the total  
330 CO<sub>2</sub> emission whilst the vehicle is not moving.

331  
332

333 Figure 4. Box Plots of the Test Sections gCO<sub>2</sub>/km, Average Speed and Vehicle Speed Coefficient of  
 334 Variation measurements, over the 48 Test Runs



335  
336

337

338 **4. Evaluation of the LiDAR-GIS method for Road Grade Estimation.**

339

340 As demonstrated in other studies (Coelho et al., 2009; Song and Yu, 2009; Zhai et al., 2008), CO<sub>2</sub>  
 341 emission increases approximately monotonically with positive VSP and has a consistently low CO<sub>2</sub>  
 342 emission rate with negative VSP. To evaluate whether the LiDAR-GIS road grade values enhanced  
 343 the calculation of VSP, the Pearson Correlation Coefficient (r) between VSP and CO<sub>2</sub> emission was  
 344 calculated for each of the 48 test laps, for VSP calculated both with (VSP<sub>G</sub>) and without (VSP<sub>0</sub>) the  
 345 LiDAR-GIS 1Hz road grade.

346

347 Table 1. Summary of the Pearson Correlation Coefficient (r) values between VSP and PEMS  
 348 measured CO<sub>2</sub> emission for each of the 48 test laps. VSP calculated both with (VSP<sub>G</sub>) and without  
 349 (VSP<sub>0</sub>) road grade.

Test Route	Number of Runs	VSP <sub>0</sub>		VSP <sub>G</sub>	
		Ave r	r Range	Ave r	r Range
Headingley	48	0.76	0.72 - 0.80	0.79	0.74 - 0.84

350

351 To assess if there was a significant increase in the strength of the linear association between VSP and  
 352 CO<sub>2</sub> emission with the addition of road grade the Williams' t-test for comparing two non-independent  
 353 correlations was used (Howell, 2013; Williams, 1959). Both VSP calculation methods show a  
 354 relatively strong linear correlation between VSP and CO<sub>2</sub> emission (see Table 1), however the

355 strength of the linear relationship between VSP and CO<sub>2</sub> emission increased for each of the 48 test  
356 laps with the addition of the LiDAR-GIS road grade. In each instance, at a significance level of  $\alpha$   
357 =.05 (two-tailed), the correlation using VSP<sub>G</sub> proved significantly greater than the correlation  
358 calculated with VSP<sub>0</sub>, which suggests that the LiDAR-GIS method provides a reliable representative  
359 1Hz gradient.

360

361

## 362 **5. Instantaneous CO<sub>2</sub> Modelling with and without LiDAR-GIS generated Road Grade.**

363

364 The PHEM instantaneous emission model was used to calculate the second-by-second CO<sub>2</sub> emission  
365 estimates for the EURO 4 test vehicle on the Headingley test laps. In order to test the LiDAR-GIS  
366 road grade methodology, CO<sub>2</sub> emission estimates from PHEM were calculated for each test run with  
367 the test area modelled as flat with all road grade values set as zero (PHEM<sub>0</sub>), and modelled with the  
368 calculated LiDAR-GIS road grade values (PHEM<sub>G</sub>).

369

370 PHEM was configured for the specific EURO 4 test vehicle (as described in Section 2.2) with a 150kg  
371 loading and emission estimates determined from the recorded (PEMS) speed profile for each test run  
372 under the two road grade conditions specified in PHEM<sub>0</sub> and PHEM<sub>G</sub>. For each of the 48 test laps and  
373 sections the PHEM<sub>0</sub> and PHEM<sub>G</sub> modelled CO<sub>2</sub> aggregate emissions were compared with the  
374 corresponding PEMS measurements (illustrated in the Figure 5 boxplots). Modelling each of the 48  
375 test laps, the average PHEM<sub>G</sub> estimate of the lap total CO<sub>2</sub> emission was 91% of the real-world PEMS  
376 measured CO<sub>2</sub> emission, with a range from 81% to 110% (with 50% of the PHEM<sub>G</sub> estimates between  
377 87.4% and 96.1%).

378

379 Although PHEM<sub>G</sub> modelling appears to underestimate the real-world vehicle CO<sub>2</sub> emission, which  
380 may result from the PHEM EURO 4 petrol average engine emission map not being specific to the test  
381 vehicle and/or possible disparity in the timing of the modelled and real-world gear changes, much of  
382 this discrepancy is likely to be caused by factors not included in the modelling such as day-to-day  
383 variation in ambient temperature, starter battery state of charge and use of the vehicles air  
384 conditioning and heating systems, each of which can have a significant effect on vehicle fuel  
385 consumption (Mock et al., 2012). Inaccuracy of the simulated vehicle weight may also have had an  
386 influence on the modelled rate of CO<sub>2</sub>. Although the test vehicle's kerbweight is recorded in the  
387 vehicle's specification, and the vehicle loading was estimated, the actual weight of the test vehicle  
388 was not directly measured. Future modelling would be improved by an accurate measure of the test  
389 vehicle weight, since an underestimation may result in lower modelled than measured CO<sub>2</sub> emission.

390

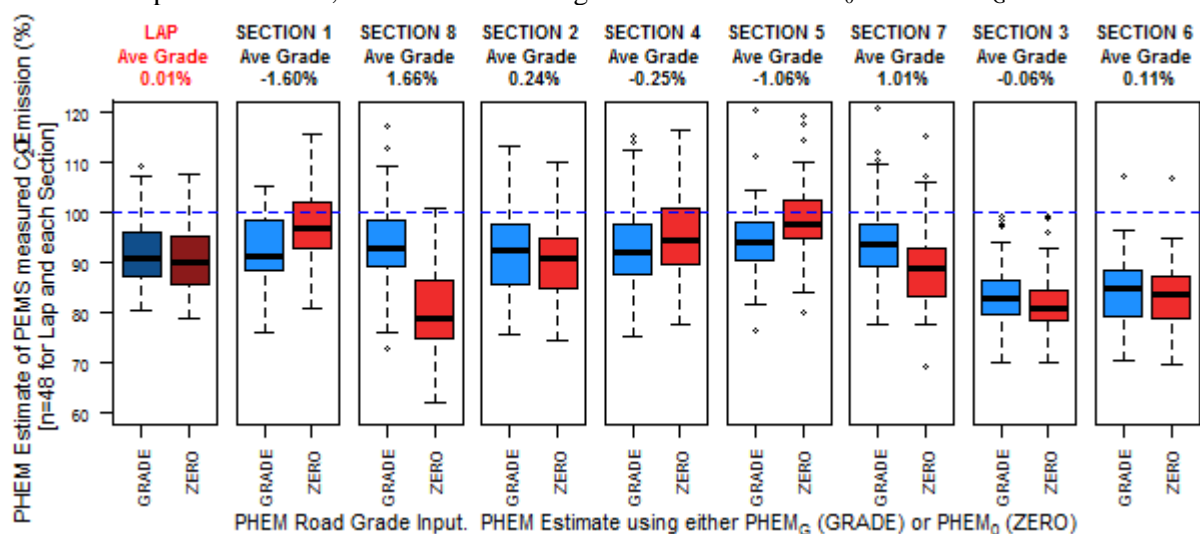
391 The average PHEM<sub>0</sub> estimate (without road grade) of the lap total CO<sub>2</sub> emission was 90% of the  
 392 PEMS recorded value, with a range from 79% to 108% (with 50% of the values between 85.8% and  
 393 95.3%). The results for the test lap are similar to those attained with PHEM<sub>G</sub>, with only a slight  
 394 improvement in PHEM CO<sub>2</sub> emission estimation over the test lap using the LiDAR-GIS road grade.  
 395 The Headingley test lap starts and ends at the same point, therefore the average road grade over the  
 396 lap is approximately zero. As a result, PHEM<sub>0</sub> overestimates of CO<sub>2</sub> emission on downhill road  
 397 segments are partially offset underestimation on uphill road segment. The overestimation /  
 398 underestimation by PHEM<sub>0</sub> can be seen in the Figure 5 test section box plots. Whilst the average  
 399 PHEM<sub>G</sub> estimate of the PEMS CO<sub>2</sub> emission in Sections 1, 2, 4, 5, 7 and 8 (excluding the turning  
 400 sections) range between 91% and 94%, the PHEM<sub>0</sub> estimates of PEMS CO<sub>2</sub> emission are greatly  
 401 influenced by the road grade in the section and vary from 79% to 98%.

402

403 For example over Section 1, a primarily downhill section with an average road grade of -1.6%, the  
 404 average PHEM<sub>G</sub> and PHEM<sub>0</sub> estimates of the section total CO<sub>2</sub> emission were 91% and 97% PEMS  
 405 measured emission respectively. In this instance the PHEM<sub>0</sub> appears to provide the most accurate  
 406 estimate of the real-world CO<sub>2</sub> emission. However over Section 8, the corresponding uphill section  
 407 (the opposite traffic flow to Section 1) the average total section CO<sub>2</sub> emission estimate from PHEM<sub>0</sub>  
 408 is 79% of the PEMS measured value, whereas for PHEM<sub>G</sub> it is 93%. Whilst the calculated PHEM<sub>0</sub>  
 409 CO<sub>2</sub> emissions for the downhill sections (1, 4 and 5) are closer to the PEMS measured emission, the  
 410 stability of the PHEM<sub>G</sub> estimates over all sections irrespective of average road grade demonstrates the  
 411 addition of the LiDAR-GIS data in PHEM delivers consistently more reliable micro-simulation CO<sub>2</sub>  
 412 emission estimates.

413

414 Figure 5. PHEM modelled CO<sub>2</sub> emission as a percentage of the PEMS measured emission for each of  
 415 the 48 test laps and sections, under the two road grade scenarios PHEM<sub>0</sub> and PHEM<sub>G</sub>.



416

417

418 The PHEM CO<sub>2</sub> emission estimates of the real-world emission through the short ‘turning’ sections 3  
419 and 6 are perceptibly less accurate than for the longer test sections. The decrease in the accuracy of  
420 PHEM in these sections is likely to be due to the driver gear selections in these short stop start  
421 sections not being characteristic of the gear shift patterns under normal driving conditions and hence  
422 not being adequately represented in the model.

423

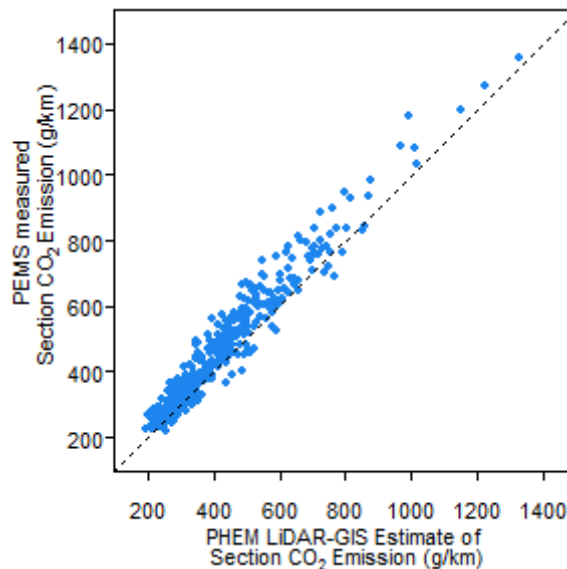
424 The stability and accuracy of the PHEM<sub>G</sub> estimates when compared to the measured PEMS CO<sub>2</sub>  
425 emission at this micro-scale section level suggests that both the LiDAR-GIS method for generating  
426 road grade provides a representative 1Hz gradient profile and that reliable micro-scale simulation of  
427 CO<sub>2</sub> emission over real-world networks is possible utilising the PHEM power-instantaneous emission  
428 model.

429

430 The scatter plot of PHEM<sub>G</sub> CO<sub>2</sub> emission estimate versus the PEMS measured CO<sub>2</sub> emission for each  
431 section (n=348) (see Figure 6) demonstrates the strength of the PHEM<sub>G</sub> model in estimating the real-  
432 world vehicle CO<sub>2</sub> emission over the Headingley test sections.

433

434 Figure 6. PHEM<sub>G</sub> Calculated gCO<sub>2</sub>/km Emission versus PEMS Recorded gCO<sub>2</sub>/km Measurements  
435 for the Headingley Test Sections.



436

437

438

## 439 6. Sensitivity of CO<sub>2</sub> Emission Estimates to Road Grade

440

441 The sensitivity of the CO<sub>2</sub> emission predictions to road grade was tested by lessening and  
442 exaggerating the gradient profiles. PHEM CO<sub>2</sub> emission estimates for the test vehicle were calculated  
443 using the real-world PEMS measured speed profiles under five road grade scenarios, where  
444 coefficients of 0, 0.5, 1, 2 and 3 were applied respectively to each second of LiDAR-GIS calculated  
445 road grade. The zero road grade coefficient (PHEM<sub>0</sub>) models the test area as totally flat. With the 0.5

446 coefficient (PHEM<sub>0.5G</sub>), the model uses half of the calculated LiDAR-GIS value at each second. For  
447 PHEM<sub>0.5G</sub> 96.79% of the 1Hz road grade estimates were between  $\pm 2\%$  with 99.61% between  $\pm 3\%$ .  
448 For PHEM<sub>G</sub> 99.46% of the 1Hz road grade estimates were between  $\pm 6\%$  and 94.4% were within the  
449 range of  $\pm 4\%$ . Doubling the road grade at each section with the road grade coefficient of 2 (PHEM<sub>2G</sub>),  
450 76.24% of the 1Hz road grade estimates were between  $\pm 6\%$  and 97.46% were within the range of  
451  $\pm 10\%$ . With a road grade coefficient set to 3 (PHEM<sub>3G</sub>) 80.93% of the 1Hz road grade estimates were  
452 between  $\pm 10\%$  and 96.26% were within the range of  $\pm 14\%$  Whilst it is likely that in real-world  
453 driving the steeper road grades would have an impact on the speed profile of the vehicle, to enable  
454 comparison, the modelling in this section of the study assumes the same speed profiles (as measured  
455 by the PEMS system) for the vehicle at every road grade coefficient.

456

457 Table 2 details the PHEM modelled CO<sub>2</sub> emission results for the 48 test runs over each lap and  
458 section for the 5 road grade scenarios. The average lap CO<sub>2</sub> emission under PHEM<sub>0</sub> is 400 gCO<sub>2</sub>/km  
459 with a range over the 48 test runs from 276 – 513 gCO<sub>2</sub>/km. The average lap CO<sub>2</sub> emission increase  
460 by 1.4% when the LiDAR-GIS road grade (PHEM<sub>G</sub>) is considered. For PHEM<sub>2G</sub> the average CO<sub>2</sub>  
461 emission change over the lap compared to PHEM<sub>0</sub> is 4.0% higher, rising to +7.6% for the PHEM<sub>3G</sub>  
462 scenario. As this test lap starts and ends at approximately the same point, the average lap road grade is  
463 zero. This modelling suggests that it is incorrect to assume that over a test route with an average flat  
464 road grade but which experiences change in elevation over the length of its profile, that the increase in  
465 CO<sub>2</sub> emission in uphill sections will be offset by the decrease in CO<sub>2</sub> emission in downhill sections.  
466 The PHEM modelling indicates that for such test routes CO<sub>2</sub> emission increases with increasing  
467 steepness of road grade.

468

469 Analysing the PHEM calculations at the section micro-scale suggests that road grade is a very  
470 important factor in establishing CO<sub>2</sub> emission over short road sections. Over Section 8, a relatively  
471 fast free flowing uphill section (with an average road grade of +1.66% from the LiDAR-GIS elevation  
472 profile), the average increase in CO<sub>2</sub> emission from PHEM<sub>0</sub> to PHEM<sub>G</sub> is 17.2% with a range in CO<sub>2</sub>  
473 emission increase for the section of between 8.5% and 43.2%. Over the same section under PHEM<sub>3G</sub>,  
474 with a hypothetical tripling of 1Hz road grade, the CO<sub>2</sub> emission increase range is from 32.3% to  
475 102.1%. This suggests conducting micro-scale modelling without establishing accurate road grade  
476 would cause the CO<sub>2</sub> emission estimates to vary considerably from the real-world CO<sub>2</sub> emission.

477



478 Table 2. PHEM CO<sub>2</sub> Emission Calculation under five road grade scenarios.

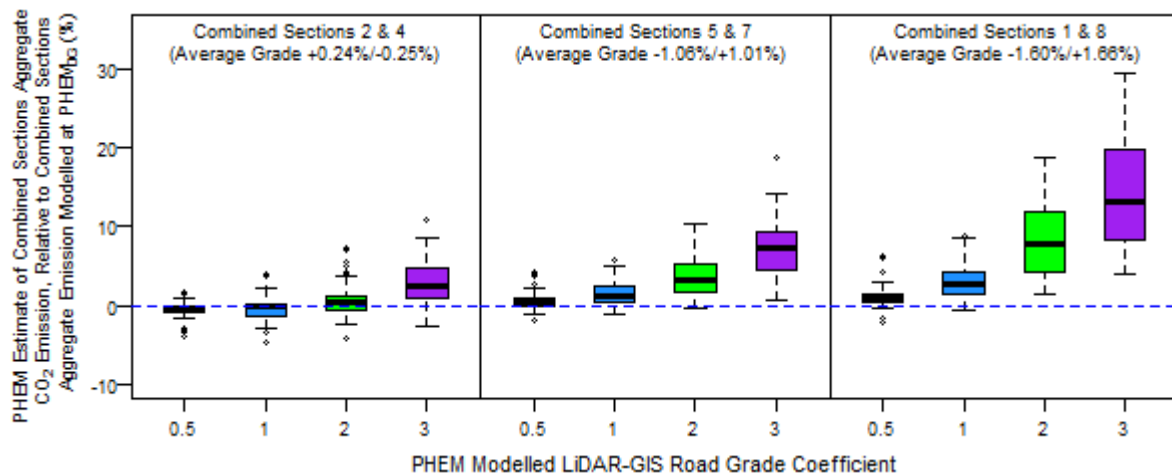
CO <sub>2</sub> Emission Comparison at Modelled Road Grade Coefficients											
Section #	Ave. Grade (%)	PHEM <sub>0</sub>		PHEM <sub>0.5G</sub>		PHEM <sub>G</sub>		PHEM <sub>2G</sub>		PHEM <sub>3G</sub>	
		Ave. (g/km)	Range (g/km)	Ave. (% Change from PHEM <sub>0</sub> )	Range (% Change from PHEM <sub>0</sub> )	Ave. (% Change from PHEM <sub>0</sub> )	Range (% Change from PHEM <sub>0</sub> )	Ave. (% Change from PHEM <sub>0</sub> )	Range (% Change from PHEM <sub>0</sub> )	Ave. (% Change from PHEM <sub>0</sub> )	Range (% Change from PHEM <sub>0</sub> )
1	-1.60	509	210 - 1037	-2.7	-9.3 - 0.3	-4.8	-11.7 - -3.9	-8.0	-17.5 - -3.9	-9.9	-22.2 - -4.5
8	1.66	258	170 - 336	8.5	4.0 - 32.0	17.2	8.5 - 43.2	37.1	18.5 - 67.7	57.1	32.3 - 102.1
2	0.24	274	203 - 503	0.5	-4.7 - 3.7	2.0	-3.8 - 11.0	4.8	-1.7 - 13.9	8.7	1.0 - 17.5
4	-0.25	409	236 - 876	-1.4	-6.3 - 2.7	-2.0	-6.7 - 5.3	-2.3	-7.1 - 7.6	-1.5	-6.7 - 8.3
5	-1.06	434	246 - 1322	-2.4	-7.5 - 1.1	-4.1	-9.7 - 2.3	-7.4	-17.8 - 0.7	-9.1	-20.7 - 3.3
7	1.01	515	257 - 856	3.2	0.9 - 12.9	6.0	2.0 - 17.2	12.1	5.1 - 28.2	20.1	8.3 - 41.0
3	0.06	436	273 - 986	0.7	-1.1 - 2.6	1.7	-0.5 - 6.3	3.9	0.0 - 8.9	7.0	0.5 - 14.3
6	0.11	524	344 - 957	0.4	-3.5 - 3.9	0.9	-3.3 - 2.0	2.4	-2.3 - 6.5	4.4	-0.4 - 9.4
LAP	0.01	400	276 - 513	0.5	-0.8 - 2.3	1.4	-0.3 - 3.9	4.0	1.4 - 8.9	7.6	3.2 - 15.8

479

480 In order to assess how the magnitude of CO<sub>2</sub> emission varies with road grade over a road segment  
 481 with two-way traffic flow, the total CO<sub>2</sub> emission over paired sections 1 and 8, 5 and 7, 2 and 4 were  
 482 calculated. The total CO<sub>2</sub> emission was calculated over each combined section for each of the 48 test  
 483 runs under the five road grade scenarios. As these section pairs cover the same road segment there is  
 484 no net change in elevation, so the average grade of each of the combined sections is zero. In Figure 7,  
 485 the combined sections aggregate CO<sub>2</sub> emissions for each of the road grade coefficients (0.5, 1, 2 and 3)  
 486 are referenced against the aggregate CO<sub>2</sub> emission over the same combined section with PHEM<sub>0G</sub>. The  
 487 results indicate that the higher CO<sub>2</sub> emissions on uphill sections are not offset by the lower emission  
 488 rates on downhill sections. The discrepancy over the combined sections tends to rise as the road  
 489 grade coefficient applied in the PHEM modelling increases. The magnitude of the increase in  
 490 emission is greatest where the average road grades of the two sections of opposing traffic flow are  
 491 steepest.

492

493 Figure 7. Percentage Change in the PHEM Aggregate Total CO<sub>2</sub> Emission between PHEM<sub>0G</sub> and  
 494 PHEM<sub>G</sub> modelled with each Road Grade Coefficient, over the Combined Sections.



495

496  
497  
498  
499  
500  
501  
502  
503  
504  
505  
506  
507  
508  
509  
510  
511  
512  
513  
514  
515  
516  
517  
518  
519  
520  
521  
522  
523  
524  
525  
526  
527  
528  
529  
530  
531

It should be noted that the traffic conditions in the road sections that make up the combined pairs can be quite different for each direction of traffic flow, as traffic control measures and traffic volume can cause different levels of congestion, resulting in a wide range of CO<sub>2</sub> emission values in each section (as illustrated in Figure 4). However the results in Figure 7 present the calculated emission from real-world speed profiles recorded throughout the day, and thus these combined emissions should reflect the likely range of CO<sub>2</sub> emission for the test vehicle on these real-world road segments.

## 7. Summary and Conclusions

Analysis of the PEMS data revealed a wide spectrum of traffic flow conditions captured by the instrumented vehicle repeatedly driving through the urban traffic network, with measurements taken both during peak rush hour congestion and in free flowing traffic conditions. A wide range of CO<sub>2</sub> emission values were recorded (PEMS) over the test lap, ranging from 313 gCO<sub>2</sub>/km to 586 gCO<sub>2</sub>/km. The measured CO<sub>2</sub> emission values were consistently higher than those predicted by the UK EFT average speed emission curve. The spread of the CO<sub>2</sub> emission values at each speed demonstrates why average speed based emission models may not reliably predict CO<sub>2</sub> emission estimates for short road segments/ sections as they fail to correctly account for acceleration, road grade, drag, rolling resistance and engine speed.

This study has shown that in order to accurately estimate vehicle CO<sub>2</sub> exhaust emissions at a micro-scale in real-world conditions, a representative road grade profile for each second of the test data is needed. The straightforward and quick LiDAR-GIS method proposed in this study provides a methodology for determining road grade for each second of a vehicle journey, and improved the modelling of CO<sub>2</sub> emission for this PEMS data set. The research demonstrates that using the PHEM instantaneous emission model with LiDAR-GIS calculated road grade is a viable method for generating accurate real-world micro-scale CO<sub>2</sub> emission estimates. The results also show that it is incorrect to assume that the increase in emission on uphill sections will be offset by the decrease in emission on paired downhill sections.

The research shows that failing to account for even a relatively modest road grade, when modelling micro-scale vehicle emission, could potentially result in highly inaccurate estimates of real-world emission. Transport management and urban planning projects should be incorporating road grade into their analysis where prediction of vehicle emissions is required.

532 With the proposal for a PEMS element in Euro 6c type approval from September 2017 (Delphi, 2013)  
533 the development of a robust yet practical road grade estimation methodology for PEMS analysis will  
534 be very important to assist the analysis of on-road test data and quantify the relationship between  
535 power output and exhaust emission. Whilst this research focused on CO<sub>2</sub> emission, it is expected that  
536 road grade will have an even greater influence on the emission of other exhaust pollutant such as NO<sub>x</sub>  
537 where a higher proportion of emissions are related to high power events (Carslaw et al, 2013).

538

539

## 540 **Acknowledgements**

541

542 David Wyatt is supported by the Doctoral Training Centre in Low Carbon Technologies at the  
543 University of Leeds funded through the UK EPSRC. Thanks go to Bob Boreham for his help in the  
544 instrumentation of the test vehicle and driving. The PEMS data used in this research was recorded as  
545 part of the EPSRC research grant, GR/S31126/01, for the RETEMM (Real-world Traffic Emissions  
546 Measurement and Modelling) Project.

547

548

## 549 **References**

550

551 Bluesky,2013. LiDAR Height Data. <http://www.bluesky-world.com/products/lidar/>, 05/11/2013.

552

553 Boriboonsomsin, K., Barth, M., 2009. Impacts of Road Grade on Fuel Consumption and Carbon  
554 Dioxide Emissions Evidenced by Use of Advanced Navigation Systems. Transportation Research  
555 Record(2139), 21-30.

556

557 Boroujeni, B.Y., Frey, H.C., 2014. Road grade quantification based on global positioning system data  
558 obtained from real-world vehicle fuel use and emissions measurements. Atmospheric Environment  
559 85(0), 179-186.

560

561 Boroujeni, B.Y., Frey, H.C., Sandhu, G.S., 2013. Road Grade Measurement Using In-Vehicle, Stand-  
562 Alone GPS with Barometric Altimeter. Journal of Transportation Engineering-Asce 139(6), 605-611.

563

564 Coelho, M.C., Frey, H.C., Roupail, N.M., Zhai, H., Pelkmans, L., 2009. Assessing methods for  
565 comparing emissions from gasoline and diesel light-duty vehicles based on microscale measurements.  
566 Transportation Research Part D-Transport and Environment 14(2), 91-99.

567

568 Daham, B., Andrews, G.E., Li, H., Ballesteros, R., Bell, M.C., Tate, J., Ropkins, K., 2005.  
569 Application of a Portable FTIR for Measuring On-road Emissions. SAE International.

570

571 DEFRA,2009. Emission Factors Toolkit for Vehicle Emissions. [http://laqm.defra.gov.uk/review-and-](http://laqm.defra.gov.uk/review-and-assessment/tools/emissions.html#eft)  
572 [assessment/tools/emissions.html#eft](http://laqm.defra.gov.uk/review-and-assessment/tools/emissions.html#eft), 11/10/2013.

573

574 Delphi, 2013. Worldwide Emission Standards: Passenger Cars and Light Duty Vehicles 2013/2014.  
575 delphi.com/emissions-pc.

576

577 Doucette, R.T., McCulloch, M.D., 2011. Modeling the CO<sub>2</sub> emissions from battery electric vehicles  
578 given the power generation mixes of different countries. *Energy Policy* 39(2), 803-811.  
579

580 Ehsani, M., Gao, Y., Emadi, A., 2009. *Modern electric, hybrid electric, and fuel cell vehicles :  
581 fundamentals, theory, and design*, 2nd ed. ed. CRC ; London : Taylor & Francis [distributor], Boca  
582 Raton, Fla.  
583

584 Ford, 2005. Ford Motor Company Limited. *The New Ford Mondeo. Brochure*. Published by Ford  
585 Motor Company Limited, Brentwood, Essex, England; May 2005.  
586

587 Frey, H.C., Unal, A., Roupail, N.M., Colyar, J.D., 2003. On-road measurement of vehicle tailpipe  
588 emissions using a portable instrument. *Journal of the Air & Waste Management Association* 53(8),  
589 992-1002.  
590

591 GPSVisualizer,2013. GPS Visualizer Website. <http://www.gpsvisualizer.com/>, 07/10/2013.  
592

593 Hausberger, S., 2003. *Simulation of Real World Vehicle Exhaust Emissions. VKM-THD Mitteilungen;  
594 Heft/Vol 82; Verlag der Technischen Universitat Graz 2003, ISBN 3-901351-74-4.*  
595 Hausberger, S., REXIS, M., Zallinger, M., Luz, R., 2010. *PHEM User Guide for Version 10.*  
596 Technische Universitat Graz.  
597

598 Howell, D.C., 2013. *Statistical methods for psychology*, Eighth edition, International edition. ed.  
599 Jimenez-Palacios, J., 1999. *Understanding and quantifying motor vehicle emissions with vehicle  
600 specific power and TILDAS remote sensing*, Doctoral Dissertation, Department of Mechanical  
601 Engineering, Massachusetts Institute of Technology, Cambridge, MA.  
602

603 Koupal, J., Nam, E., Giannelli, B., Bailey, C., 2004. *The MOVES Approach to Modal Emission  
604 Modeling*. Presented at the 14th CRC On-Road Vehicle Emissions Workshop, San Diego, CA.  
605

606 Li, H., Andrews, G.E., Savvidis, D., Daham, B., Ropkins, K., Bell, M., Tate, J., 2008. *Study of  
607 Thermal Characteristics and Emissions during Cold Start using an on-board Measuring Method for  
608 Modern SI Car Real World Urban Driving*. *SAE Int. J. Engines* 1(1), 804-819.  
609

610 Liu, H.A., Barth, M., Scora, G., Davis, N., Lents, J., 2010. *Using Portable Emission Measurement  
611 Systems for Transportation Emissions Studies Comparison with Laboratory Methods*. *Transportation  
612 Research Record*(2158), 54-60.  
613

614 Millin-Chalabi, G., Schumm, J., Gupta, B., Tun, Y., Kandeh, J., Kitmitto, K., 2011. *The Landmap  
615 Service: Reaching New Horizons in Data Management and E-Learning*. RSPSoc Annual Conference  
616 2011, Bournemouth University, UK.  
617

618 Mock, P., German, J., Bandivadekar, A., Riemersma, I., 2012. *Discrepancies between type-approval  
619 and "real-world" fuel-consumption and CO<sub>2</sub> values. Assessment for 2001-2011 European passenger  
620 cars*. ICCT Working Paper; April 2012. Paper no 2012-2.  
621

622 Nakamura, H., Kihara, N., Adachi, M., Ishida, K., 2002. *Development of a Wet-based NDIR and Its  
623 Application to On-board Emission Measurement System*. SAE International.  
624 Racelogic,2008. *VBOX II Lite 5Hz GPS Data Logger User Guide*.  
625 [http://www.racelogic.co.uk/downloads/vbox/Manuals/Data\\_Loggers/RLVB2L\\_Manual.pdf](http://www.racelogic.co.uk/downloads/vbox/Manuals/Data_Loggers/RLVB2L_Manual.pdf),  
626 30/06/2014.  
627

628 Ropkins, K., Quinn, R., Beebe, J., Li, H., Daham, B., Tate, J., Bell, M., Andrews, G., 2007. *Real-  
629 world comparison of probe vehicle emissions and fuel consumption using diesel and 5% biodiesel (B5)  
630 blend*. *Science of the Total Environment* 376(1-3), 267-284.  
631

- 632 Ropkins, K., Tate, J.E., Li, H., Andrews, G.E., Hawley, G., Bell, M.C., 2008. Chassis Dynamometer  
633 Evaluation of On-board Exhaust Emission Measurement System Performance in SI Car under  
634 Transient Operating Conditions. SAE International.  
635
- 636 Sahlholm, P., Johansson, K.H., 2010. Road grade estimation for look-ahead vehicle control using  
637 multiple measurement runs. *Control Engineering Practice* 18(11), 1328-1341.  
638
- 639 Smit, R., Smokers, R., Rabe, E., 2007. A new modelling approach for road traffic emissions:  
640 VERSIT+. *Transportation Research Part D-Transport and Environment* 12(6), 414-422.  
641
- 642 Song, G.H., Yu, L., 2009. Estimation of Fuel Efficiency of Road Traffic by Characterization of  
643 Vehicle-Specific Power and Speed Based on Floating Car Data. *Transportation Research*  
644 *Record*(2139), 11-20.  
645
- 646 Williams, E.J., 1959. The Comparison of Regression Variables. *Journal of the Royal Statistical*  
647 *Society Series B-Statistical Methodology* 21(2), 396-399.  
648
- 649 Zhai, H.B., Frey, H.C., Roupail, N.M., 2008. A Vehicle-Specific Power Approach to Speed- and  
650 Facility-Specific Emissions Estimates for Diesel Transit Buses. *Environmental Science & Technology*  
651 42(21), 7985-7991.  
652
- 653 Zhang, K.S., Frey, H.C., 2006. Road grade estimation for on-road vehicle emissions modeling using  
654 light detection and ranging data. *Journal of the Air & Waste Management Association* 56(6), 777-788.